Monthly Notices
of the
ROYAL ASTRONOMICAL SOCIETY

MNRAS **489,** 3981–3989 (2019)
Advance Access publication 2019 September 13

doi:10.1093/mnras/stz2417

Detection of new methanol maser transitions associated with G358.93−0.03

G. C. MacLeod,[1,2★] K. Sugiyama,[3★] T. R. Hunter,[4★] J. Quick,[2] W. Baan,[5] S. L. Breen,[6] C. L. Brogan,[4] R. A. Burns,[3,7] A. Caratti o Garatti,[8] X. Chen,[9,10] J. O. Chibueze,[11,12] M. Houde,[1] J. F. Kaczmarek,[13] H. Linz,[14] F. Rajabi,[15,16] Y. Saito,[17] S. Schmidl,[18] A. M. Sobolev,[19] B. Stecklum,[18] S. P. van den Heever[2] and Y. Yonekura[17]

Affiliations are listed at the end of the paper

Accepted 2019 August 22. Received 2019 August 20; in original form 2019 June 23

ABSTRACT

We report the detection of new 12.178, 12.229, 20.347, and 23.121 GHz methanol masers in the massive star-forming region G358.93−0.03, which are flaring on similarly short time-scales (days) as the 6.668 GHz methanol masers also associated with this source. The brightest 12.178 GHz channel increased by a factor of over 700 in just 50 d. The masers found in the 12.229 and 20.347 GHz methanol transitions are the first ever reported and this is only the fourth object to exhibit associated 23.121 GHz methanol masers. The 12.178 GHz methanol maser emission appears to have a higher flux density than that of the 6.668 GHz emission, which is unusual. No associated near-infrared flare counterpart was found, suggesting that the energy source of the flare is deeply embedded.

Key words: masers – stars: formation – stars: protostars – ISM: individual objects: MMB G358.931-0.030 – ISM: molecules – radio lines: ISM.

1 INTRODUCTION

Massive star formation is likely to involve episodic, disc-mediated bursts of accretion analogous to the FU Ori (Hartmann & Kenyon 1996) and EX Ori (Herbig 1977, 1989) phenomena seen in low-mass stars. The outbursts in these objects can occur over periods from weeks to decades (Audard et al. 2014). The deeply embedded nature of accreting massive protostars impedes observations and hampers direct investigation of the accretion process. However, recently, masers have emerged as a powerful tool to probe candidate accretion events. Two high-mass young stellar objects (HMYSO), NGC 6334I-MM1 (Hunter et al. 2017) and S255 IR-NIRS3 (Caratti o Garatti et al. 2017), underwent major accretion events; the former found in the millimetric range and the latter in the infrared. In both cases 6.668 GHz methanol maser flaring events were discovered serendipitously, but they occurred over time-scales of months (Fujisawa et al. 2015; MacLeod et al. 2018). At least in the case of NGC 6334I, several other transitions with detected masers, including from other species, were monitored and also flared (MacLeod et al. 2018).

As a result of a single-dish maser monitoring program, Sugiyama et al. (2019) reported a fast flaring event, rising on a time-scale of days, in the 6.668 GHz methanol masers associated with the massive star-forming region G358.93−0.03. But by all measures, G358.93−0.03 was a relatively unknown and unimpressive massive star-forming region. It was discovered via its associated 6.668 GHz methanol masers by Caswell et al. (2010). They detected a maser with $S_{6.668}$(peak) = 10 Jy at the Local Standard of Rest velocity $v_{\rm LSR} = -15.9\,{\rm km\,s^{-1}}$, after 2006 January 22 and before 2006 March 31; the velocity range of the weak emission was between −22.0 and $-14.5\,{\rm km\,s^{-1}}$. A 12.178 GHz methanol maser survey by Breen et al. (2012) found no such associated emission above 0.8 Jy. No hydroxyl masers, e.g. see Qiao et al. (2014), are reported. Weak water masers were detected by Titmarsh et al. (2016) where $S_{22\,\rm GHz} \sim 0.7$ Jy at $v_{\rm LSR} = -21.6\,{\rm km\,s^{-1}}$. Hu et al. (2016) mapped the 6.668 GHz methanol masers of the high-mass young stellar object (HMYSO) in 2012; it was only 5 Jy and had the same velocity extent as originally reported. The masers were also mapped by Rickert, Yusef-Zadeh & Ott (2019) on 2015 September 09, who identified three 6.668 GHz methanol maser features at $v_{\rm LSR} = -18$, −17, and $-16\,{\rm km\,s^{-1}}$ ($F_{6.668}$ = 1–3 Jy) in a single position.

Millimetre continuum emission from the HMYSO was reported in the Bolocam Galactic Plane Survey (BGPS) as source G358.936−0.032 (Rosolowsky et al. 2010) and in the APEX Telescope Large Area Survey of the Galaxy (ATLASGAL) as source J174311.2−295129 (Contreras et al. 2013). Urquhart et al. (2013) reported a flux density of 1.4 Jy at 870 μm. The best estimate of the kinematic distance and bolometric luminosity range of the region is described by Brogan et al. (2019) as $6.75^{+0.37}_{-0.68}$ kpc and 5700–

★ E-mail: gord@hartrao.ac.za (GCM); koichiro.sugiyama@nao.ac.jp (KS); thunter@nrao.edu (TRH)

22000 $L_\odot$. These authors present recent Atacama Large Millimeter Telescope (ALMA) and Submillimeter Array (SMA) data which reveal two hot molecular cores (MM1 and MM3 separated by about 1″.25), with the richer core exhibiting unprecedented (sub)millimetre methanol maser emission including torsionally excited ($v_t = 1$ and 2) methanol transitions. They state that the brightness temperatures are high implying that these are masers and not thermal emission lines. The thermal methanol emission towards this core peaks at $-16.5\,km\,s^{-1}$ with a linewidth of $3.1\,km\,s^{-1}$.

The Maser Monitoring Organisation (M2O), including its voluntary group of observatories who monitor masers, was alerted to the rapidly strengthening 6.668 GHz methanol masers associated with G358.93−0.03 (Sugiyama et al. 2019). Breen et al. (2019) amazingly discovered several never-before detected methanol maser transitions including torsionally excited ($v_t = 1$) methanol transitions. We present confirmatory 6.668 GHz methanol maser observations and the results of searches for hydroxyl, formaldehyde, water, and methanol masers associated with G358.93−0.03 using the Hartebeesthoek Radio Astronomy Observatory (HartRAO). We also report the discovery of rare 23.121 GHz methanol masers along with never-before detected masers in two other methanol transitions.

2 OBSERVATIONS

2.1 Hartebeesthoek Radio Astronomy Observatory

Observations using the 26 m telescope of Hartebeesthoek Radio Astronomy Observatory (HartRAO)[1] were made in four receiver bands. The 1.3, 4.5, 5.0, and 18.0 cm receivers are each dual, left (LCP) and right (RCP), circularly polarized, cryogenically cooled receivers; the 2.5 cm receiver was uncooled. Each receiver and polarization were calibrated independently relative to Hydra A and 3C 123, assuming the flux scale of Ott et al. (1994) (Jupiter was also observed for the 1.3 cm receiver data). The point source sensitivity (PSS) for the 1.3 and 2.5 cm receivers are 10.5 and 5.8 $Jy\,K^{-1}$ per polarization; for the 4.5, 5.0, and 18.0 cm receivers it is 5.1 $Jy\,K^{-1}$ per polarization. The beamsize of the 1.3, 2.5, 4.5, 5.0, and 18.0 cm receivers are 2′.1, 4′.0, 7′.0, 7′.5, and 29′.6, respectively. For all receivers, except the 1.3 cm receiver, observations were completed in frequency switching mode and a 1.0 MHz bandwidth on the 1024-channel (per polarization) spectrometer. Observations made with the 1.3 cm receiver employed position switching and a 2.0 MHz bandwidth. Also half-power beamwidth pointing correction observations were completed for all epochs of observation except for the 18.0 cm observations. More information for each receiver and the observing method employed are described in MacLeod et al. (2018).

The observations performed on 2019 January 21 included an attempt to confirm reports of the 6.668 GHz methanol flare (Sugiyama et al. 2019), and an exploratory investigation of the 12.178 and 23.121 GHz lines. The velocity resolution of the 6.668, 12.178, and 23.121 GHz observations are 0.044, 0.048, and 0.101 $km\,s^{-1}$, respectively. Monitoring began on 2019 January 25 and at a cadence of 1 to 3 d thereafter. Each monitoring epoch of observation is comprised of two 6 min observations.

Prompted by our experience with NGC 6334I (MacLeod et al. 2018), we also searched for associated hydroxyl (1.665, 1.667, 1.720, 1.612, 4.660, 4.765, 6.031, 6.035, and 6.049 GHz), formaldehyde (4.830 GHz), and water (22.235 GHz) masers. The 1.665 GHz OH transition was first observed on 2019 January 20 and at another seven epochs with the last on 2019 May 08; the others were observed between 2019 February 16 and March 25. The 4.830 GHz formaldehyde transition was observed only once on 2019 February 17. Hydroxyl and formaldehyde observations were completed as described in MacLeod et al. (2018).

Encouraged by the detection of new 12.178 GHz masers and very rare 23.121 GHz masers, we systematically searched for other new methanol transitions (83) in the available receivers described above beginning on 2019 March 12. Two new transitions with detectable masers, 12.229 and 20.347 GHz were discovered on 2019 March 12 with a velocity resolution of 0.048 and 0.115 $km\,s^{-1}$, respectively. For the 20.347 GHz transition we observed using rest frequencies 20.346846 GHz (provided by the Jet Propulsion Laboratory; Pickett et al. 1998) and 20.346830 GHz (F. J. Lovas, private communication and Remijan, Markwick-Kemper & ALMA Working Group on Spectral Line Frequencies 2007). We selected the latter because the spectra better matched the 6.668 and 12.178 GHz methanol transition spectra. Monitoring of these transitions began shortly thereafter; results from this monitoring will be reported in a forthcoming paper. Transition information for each new maser is included in Table 1. Information of the non-detections (81) are listed in Table A1. The central frequencies observed were chosen predominantly from the list of transitions from tables made available by the Jet Propulsion Laboratory (Pickett et al. 1998). Some were selected from two other sources: the Cologne Database for Molecular Spectroscopy (CDMS; Müller et al. 2005) and from Lovas (2004). The uncertainty in the absolute flux density for all transitions was less than 6 per cent.

2.2 Tianma Radio Telescope

One service afforded by the M2O is to confirm new detections using different observatories. The 12.229 GHz methanol masers were thus observed using the Shanghai 65 m Tianma Radio Telescope (TMRT) on 2019 March 13; a day after the HartRAO discovery. A cryogenically cooled Ku-band receiver and digital backend system employing a 32 768 channel spectral window yielding a velocity resolution of $\sim 0.018\,km\,s^{-1}$ was used to obtain a typical rms noise of ∼0.1 Jy per spectral channel. The beamsize was ∼1′.5. The uncertainty of the absolute flux density was less than 5 per cent.

2.3 Australia telescope compact array

Likewise, the Australia Telescope Compact Array (ATCA) observed this source on 2019 April 11 at the methanol line frequency of 20.3468300 GHz. The ATCA was in the 750C array, where only antennas 1, 2, 3, and 4 were available, resulting in baseline lengths between 153 and 704 m. The Compact Array Broad-band Backend (CABB; Wilson et al. 2011) was configured in CFB 1M−0.5k mode to provide 2 MHz bandwidth with 4096 spectral channels, corresponding to a velocity coverage of 29 and $0.007\,km\,s^{-1}$ velocity channels. Observations of G 358.931−0.030 were interspersed with observations of nearby phase calibrator B 1714−336 every 10 min, and the pointing was corrected every ∼50 min of observations. PKS B 1253−055 and PKS B 1934−638 were observed for bandpass and primary flux density calibration, respectively. The observations were conducted over a period of 6 h, resulting in a total integration time of ∼2.5 h on G 358.931−0.030 and a synthesized beam of 13.0 × 2.14 arcsec. Data were reduced using MIRIAD (Sault, Teuben & Wright 1995) following the procedure outlined in Breen

[1]See http://www.hartrao.ac.za/spectra/ for further information.

Table 1. Information on the flaring maser transitions associated with G358.93−0.03. We determine, the peak, observation date of peak, the onset period, and increase factor in the selected velocity channels for each transition. We demarcate in boldface the MJD date where the flare reaches a maximum in each velocity channel we use to determine the average time lag.

Molecule	Transition Energy level	Freq.	Velocity extent v_{min}	v_{max}	v_{chan}	Velocity channel information F_{peak}	MJD_{peak}	Onset period	Increase factor
		(GHz)	(km s^{-1})	(km s^{-1})	(km s^{-1})	(Jy)	(+50 000)	(d)	
CH_3OH	$5_1 \longrightarrow 6_0\ A^+\ (v_t = 0)$	6.668[1]	− 20.2	− 13.9	− 17.4	1156	**8553**	49	66
		–	–	–	− 16.3	615	8547	43	50
		–	–	–	− 15.8	828	**8531**	25	27
		–	–	–	− 15.6	589	8573	71	17
CH_3OH	$2_0 \longrightarrow 3_{-1}\ E\ (v_t = 0)$	12.178[1]	− 20.5	− 13.6	− 17.2	1270	**8554**	50	733.5
		–	–	–	− 16.3	1256	8546	42	223.4
		–	–	–	− 15.8	1101	**8530**	26	35.0
		–	–	–	− 15.6	816	8546	42	43.6
CH_3OH	$16_5 \longrightarrow 17_4\ E\ (v_t = 0)$	12.229[2]	− 17.9	− 15.0	− 17.3	1143	**8572**	16	3.2
		–	–	–	− 15.5	1344	**8557**	1	1.1
CH_3OH	$17_6 \longrightarrow 18_5\ E\ (v_t = 0)$	20.347[2]	− 17.8	− 14.6	− 17.2	136	**8590**	34	7.0
		–	–	–	− 15.3	549	**8563**	7	1.1
CH_3OH	$9_2 \longrightarrow 10_1\ A^+\ (v_t = 0)$	23.121[1]	− 20.2	− 14.0	− 17.3	105	**8556**	51	207.2
		–	–	–	− 16.0	60	8529	24	8.8
		–	–	–	− 15.6	73	**8520**	15	7.7
		–	–	–	− 15.3	102	8568	63	44.9
H_2O	$6_1 \longrightarrow 5_2\ (F = 5 \longrightarrow 4,\ v = 0)$	22.235[1]	− 20.2	− 14.0	− 17.4	42	8595	<21	∼45

Note. [1]from the catalogue of Lovas (2004) and [2]from the JPL Line Catalogue (Pickett et al. 1998).

et al. (2019). First a flux model was fit to the PKS B1253−055 continuum band data, which was then bootstrapped to PKS B1934−638 for absolute flux density calibration. The observations had sufficient parallactic angle coverage to use B 1741−312 to calculate the leakage solution and we estimate that the polarization calibration is accurate to within ∼0.1 per cent of Stokes I. The absolute flux density calibration is expected to be accurate to within 10 per cent.

2.4 MPG/ESO 2.2m telescope

Optical and near-infrared (NIR) imaging of G358.93−0.03 was performed employing the seven-channel Gamma-ray Burst Optical/Near-infrared Detector (GROND; Greiner et al. 2008), using director's discretionary time (DDT) at the MPG/ESO 2.2 m telescope at La Silla (Chile) on 2019 February 08 (Programme number 0103.C-9033(A)). GROND records imaging data in seven filters (optical: Sloan g' r' i' z' , near-infrared: J H Ks) simultaneously. The total integration time amounts to 38 min. Data processing was performed using the GROND pipeline (Krühler et al. 2008).

3 RESULTS

3.1 Non-detections

We searched a number of transitions of OH (10), H_2CO (1), $CH_3{}^{18}OH$ (2), and CH_3OH (79) in which we found no emission. The 3σ upper limits are presented in Table A1. The 1.665 GHz OH transition was observed in eight epochs between 2019 January 20 and May 08 with no detections. The other 18 cm OH transitions were re-observed in 2019 May, but we again report no detections.

3.2 Detected methanol and water masers

We present spectra of all of the masers we detected associated with G358.93−0.03 in Fig. 1. Results of selected velocity channels of each transition are presented in Table 1. We confirm the flaring

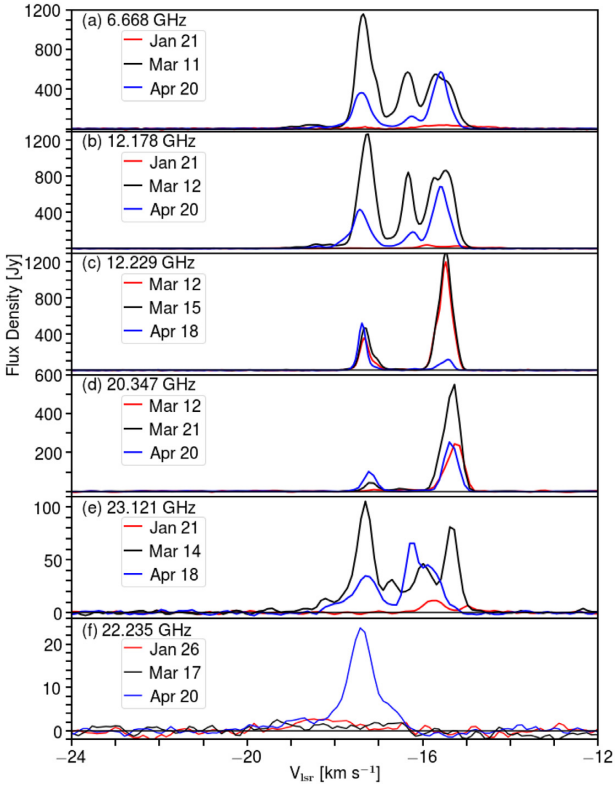

Figure 1. Selected spectra are plotted for: (a) 6.668 GHz, (b) 12.178 GHz, (c) 12.229 GHz, (d) 20.237 GHz, (e) 23.121 GHz methanol, and (f) 22.235 GHz water masers associated with G358.93−0.03.

of the 6.668 GHz methanol maser emission and its fast variation reported by Sugiyama et al. (2019) in the velocity range from −20.2 to −13.9 km s^{-1}. This velocity extent is commensurate with the original detection of 6.668 GHz methanol masers by Caswell et al.

(2010). The 12.178 and 23.121 GHz methanol spectra are similar to the 6.668 GHz methanol maser spectra. Rickert et al. (2019) mapped the 6.668 GHz emission and determined these spots were regions of maser activity; we assume here the similar 12.178 and 23.121 GHz methanol emission also represent maser emission (more on this below). These 12.178 and 23.121 GHz methanol masers are new detections towards this source. This is only the fourth object ever detected as a maser in the 23.121 GHz transition, the others being W3(OH) and NGC 7538 (Wilson et al. 1984) and NGC 6334I (Menten & Batrla 1989). For most of the velocity extent of the spectra we report that $F_{12.178} \geq F_{6.668} \geq F_{23.121}$, see the peaks listed in Table 1.

Early results of our monitoring observations are included in Table 1; the flaring continues (MacLeod et al., in preparation). During these observations we find that the emission in the brightest 6.668 GHz maser velocity channels increased by factors of between 17 and 66 in 71 d and 49 d, respectively, from 2019 January 21. The brightest velocity channel, $v_{\rm LSR} = -17.3\,{\rm km\,s^{-1}}$, for the 12.178 and 23.121 GHz methanol spectra each increased dramatically by factors of ∼700 and ∼200 in ∼50 d.

The water maser emission appears within the velocity extent presented in Titmarsh et al. (2016), and we initially detected it at a similar peak flux density level on 2019 January 26. It remained weak until flaring began between 2019 April 1 and 20; we confirm the onset of flaring reported by Xi et al. (in preparation). We estimate the water maser emission rose by a factor of ∼45.

In Fig. 1 we also present the spectra of two new methanol maser transitions, 12.229 and 20.347 GHz. These are the first such masers ever detected in these methanol transitions. The velocity extent of the 12.229 and 20.347 GHz masers are both similar to that for the 6.668 GHz masers. Their spectra are similar to each other but have only weak emission, ≤15 Jy, in the velocity range between −16 and −16.8 km s^{-1} (unlike the other methanol transitions shown here). Our observations of these lines began at about the time the 6.668 GHz methanol masers were peaking; the emission rose by factors between 1.1 and 7.0 (clearly lower limits). In summary, all three transitions are experiencing significant, contemporaneous, and fast flaring on time-scales of days.

Fortunately, observations of these new transitions were also made by others in the M2O group. We present the spectra from the TMRT (12.229 GHz) in Fig. 2 and ATCA (20.347 GHz) in Fig. 3. The TMRT spectrum at 12.229 GHz is similar but not identical to that obtained by HartRAO taken one day earlier. The brightest velocity channels at $v_{\rm LSR} = -17.3$ and $-15.4\,{\rm km\,s^{-1}}$ in the TMRT observation are about 25 per cent brighter than the interpolated values between the 2019 March 12 and 14 HartRAO observations. The difference may be the result of variability and/or differences in the calibration of each receiver. There is a slight velocity shift, ∼0.08 km s^{-1}, between the two spectra, possibly the result of slightly different transition frequencies used at each observatory. We estimate that the minimum brightness temperature for $F_{12.229}$(peak) = 1500 Jy is ∼1500 K, more than three times the transition's lower energy level (451 K). From the ATCA observations we find the temperature brightness is ∼26000 K at 20.347 GHz. Including the variability, similarity of the spectrum at different frequencies, and these estimates of the brightness temperature, we are certain the emission in each transition is maser emission.

At 20.347 GHz we find that the two brightest velocity channels found in the HartRAO data are ∼1.5 times that seen in the ATCA spectrum. We made only moderate pointing and atmospheric corrections, about 15 per cent each, to the HartRAO spectrum shown; insufficient to account for the difference. Our ongoing monitoring observations suggest that this transition peaked on 2019 March 21 and was weakening through 2019 April 13 thus suggesting the HartRAO flux density would have been greater on 2019 April 11 when the ATCA observations were taken. The ATCA observations, in the given configuration, would have included most of the extended emission. Barring significant calibration errors, it is possible that 20.347 GHz methanol masers weakened to 2019 April 11 and then rebrightened on 2019 April 13.

The ATCA observations include polarization information of the 20.347 GHz methanol masers, we present this in Fig. 3. These masers are both circularly (Stokes parameter V) and linearly (Stokes parameters Q and U) polarized. Maximum polarization is detected at $v_{\rm LSR} = -15.5\,{\rm km\,s^{-1}}$ at $V \sim 1$ per cent and $\sqrt{Q^2+U^2} \sim 4$ per cent. At $v_{\rm LSR} = -17.2\,{\rm km\,s^{-1}}$, the polarization measures are less than one per cent. This result is in line with the polarization reported in Breen et al. (2019) for several transitions including

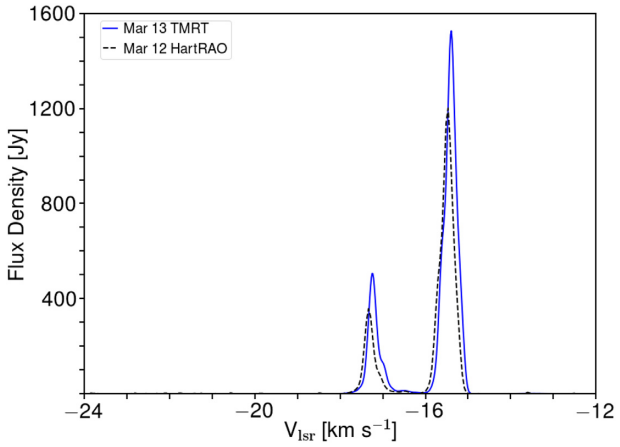

Figure 2. Spectra of 12.229 GHz methanol masers associated with G358.93−0.03 are plotted for observations obtained by TMRT on 2019 March 13 (solid blue line) and by HartRAO, nearest the TMRT observation, on 2019 March 12 (dashed black line).

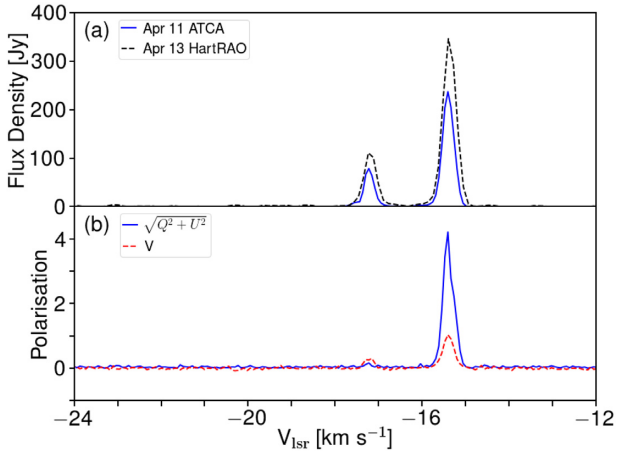

Figure 3. (a) Spectra of 20.347 GHz methanol masers associated with G358.93−0.03 are plotted for observations obtained by the ATCA on 2019 April 11 (solid blue line) and by HartRAO, nearest the ATCA observation, on 2019 April 13 (dashed black line). (b) Linear (solid blue line and circular (dashed red line) polarization data from the ATCA observations are plotted.

never-before-detected maser transitions. Breen et al. (2019) also reported that each of the new transitions they detected, including 20.347 GHz, were co-spatial with the 6.668 GHz methanol masers and all are maser emission sources.

The maxima at $v_{\rm LSR} \sim -17.3\,{\rm km\,s^{-1}}$ in the 6.668, 12.178, and 23.121 GHz transitions occurred on or about 2019 March 12 ($\rm MJD_{\it ave} = 58554 \pm 1.5$). We find that for each transition the brightest red-shifted feature reached a maximum before the brightest blue-shifted feature (MJD values used are demarcated in boldface in Table 1). We determined the average of these estimated time lags is $\tau = 22 \pm 8$ d (the uncertainty is the standard deviation).

More thorough analysis of our monitoring, and a better understanding of the evolution of this amazing flare, will be presented in a follow-up paper once the flare has subsided.

3.3 Detection of a near-infrared point source

GROND detected an NIR counterpart of the G358.93−0.03 region in the *J*, *H*, and *Ks* bands, and not at shorter wavelengths. It is known as 2MASS J17431001−2951460 (Geballe et al. 2019) and is also referred to as VVV J174310.01−295146.12 in the Data Release 2 (Minniti, Lucas & VVV Team 2017) of the VISTA Variable in the Via Lactea Survey (VVV). While 2MASS did not detect the source in the *H* band, the VVV survey reports a detection at this wavelength, with H-Ks = 3.66 mag, i.e. a very red source. In fact, a lower resolution *K* band spectrum obtained with UKIRT at epoch 2008-08-18 (Geballe et al. 2019) shows a featureless spectrum with a continuum rising towards longer wavelengths, indicative of a dust-enshrouded environment. The absence of any spectral feature precludes conclusions on its spectral type. In the VVV survey, the object has shown rapid brightness changes with a 3σ range of 0.4 mag, and a peak-to-peak variation of 0.79 mag during 5 yr of VVV *Ks*-band monitoring. The GROND photometry indicated a *Ks* brightness elevated by 0.34 mag with respect to the mean of 12.23 mag, i.e. within the range of the normal variability. Its position, to within 0.″2, is consistent with the secondary hot core and dust continuum source MM3 detected by ALMA, which is located ∼1.″1 to the southwest of the main hot core MM1 (cf. Brogan et al. 2019). Image subtraction of the latest VVV Ks frame (epoch 2015-09-19), after proper flux scaling and PSF matching, did not reveal any extended emission that would offer evidence of the existence of a light echo from an accretion outburst, unlike in the case of S255IR-NIRS3 (Caratti o Garatti et al. 2017).

3.4 Summary of results

We confirm the fast flaring nature, varying on the day scale, of the 6.668 GHz masers associated with the MMYSO G358.93−0.03. We also report the detection of new 12.178 GHz methanol maser emission, only the fourth 23.121 GHz methanol maser and that $F_{12.178} \geq F_{6.668}$. Remarkably, we discovered new masers towards this source in the 12.229 and 20.347 GHz methanol maser transitions. Observations at TMRT and ATCA confirm the existence of each, respectively. There appears to be a time lag, $\tau = 22 \pm 8$ d, between when the brightest red-shifted (peaked first) and blue-shifted velocity channels. We report no maser emission in hydroxyl, formaldehyde, and other methanol transitions. Lastly, we report little variation of the NIR emission associated with G358.93−0.03 and suggest that 2MASS J17431001−2951460 is not the IR counterpart of the alleged bursting source.

4 DISCUSSION

4.1 Temporal behaviour

It is not clear if the maser emission in velocity channels listed in Table 1 are co-propagating or co-spatial. However, there appears to be a time lag, $\tau = 22 \pm 1$ d, between the two brightest velocity channels, $v = -17.4$ and $-15.8\,{\rm km\,s^{-1}}$, in each of the transitions. At the near kinematic distance, $D_{\rm kin} \sim 6.5$ kpc, their maximum estimated separation is ∼4000 ± 200 au or 0.″6 assuming the flare is travelling at the speed of light and all transitions at the same velocity are within a few light days of each other. The projected separation of MM1 and 3 is 1.″1 (Brogan et al. 2019) while Brogan et al. and Breen et al. (2019) find the masers are associated with MM1. It is also possible that the blue-shifted feature simply has a longer coherent path-length and takes longer to reach its maximum. This argument is supported by the fact that $F_{\rm peak}(-17.3) > F_{\rm peak}(-15.8)$. More interferometric observations are required to aid our interpretation.

The 6.668 GHz methanol maser results here confirm those reported by Sugiyama et al. (2019). In fact, the flare in each transition has risen quickly to each velocity channel maximum, in at most 70 d from the start of observations, and reached flux density maxima of between $F_{23.121} = 60$ Jy to $F_{12.229} = 1340$ Jy. The fact that they are all occurring in several transitions strongly supports the hypothesis that all are amplifying a common background exciting source and possibly co-propagating. The masers associated with the HMYSOs S255 IR-NIRS3 (Fujisawa et al. 2015) and NGC 6334I (MacLeod et al. 2018) also experienced strong flares and are likely caused by accretion events as reported by Hunter et al. (2017) and Caratti o Garatti et al. (2017) respectively. The former was identified via a major increase in the millimetric dust emission while the latter was found via its NIR brightening. No evidence for millimetric brightnening (Brogan et al. 2019) nor NIR brightening (this work) has been found during this flare in G358.93−0.03.

4.2 The maser conditions

Class II masers are radiatively pumped (Sobolev & Deguchi 1994; Cragg, Sobolev & Godfrey 2005, and references therein) and found in the vicinity of HMYSOs (Breen et al. 2013, and references therein). An excellent theoretical description of the methanol molecule and its maser associated transitions is given in Sobolev, Cragg & Godfrey (1997) and Cragg et al. (2005). They predict transitions in which maser emission can occur between the levels of the highly excited ground state and torsionally excited states of methanol. Searches for several of these predicted transitions were undertaken (Cragg et al. 2001; Chipman et al. 2016; Ellingsen et al. 2011, and references therein) which brought new detections but have shown that the masers in these transitions are quite rare. Here we find no maser emission, nor thermal emission, in the Cragg et al. (2005) predicted methanol transitions at $\nu = 5.005$, 20.171, and 20.909 GHz. Perhaps the flares in these transitions had already subsided before the respective observations reported here in early 2019 March, or they did flare but at flux densities below the detection limits, $F_\nu < 2 - 4$ Jy. From the 3σ rms values above, we estimate the corresponding brightness temperature upper limits in a hypothetical 1 arcsec beam for $\nu = 5$ and 20 GHz to be $\sim 10^5$ and $\sim 10^4$ K, respectively, easily sufficient for weaker masers to lurk undetected by the single dish. Breen et al. (2019) found all the class II methanol masers they detected were co-spatial, within 0.″2, with an absolute positional accuracy of 0.″4 and associated with MM1 and the (sub)millimetre masers reported by Brogan et al. (2019).

4.2.1 Known methanol transitions

The conditions under which several class II methanol transitions are inverted, including the 6.668, 12.178, and 23.121 GHz transitions discussed here, are presented in Cragg et al. (2005, and references therein). Models in Cragg et al. (2005) predict that $F(12.178) > F(6.668)$ but only in a narrow range of conditions, i.e. the specific column density of methanol is high ($N_{meth}/\Delta V > 10^{14}$ cm^{-3} s). In dynamic regions where the conditions are changing, we might not expect the conditions for the brighter 12.178 GHz masers to exist for any significant length of time. This rarity seems confirmed by Breen et al. (2012) who found that only about three per cent of the 400 detected 6.668 GHz masers had stronger 12.178 GHz masers. They further suggest it is possible that even these examples are only the result of variability and non-simultaneous observations. MacLeod et al. (2018) did find a velocity extent in which $F(12.178) > F(6.668)$ in their near-simultaneous monitoring observations of NGC 6334I.

Here we report a clear example where the single-dish spectra of 12.178 GHz is mostly brighter than its 6.668 GHz counterpart observed within hours of each other. Likewise, the observations of the other transitions were taken within hours (or at most a day) of the 6.668 GHz masers.

4.2.2 New methanol maser transitions

Breen et al. (2019) discovered six new methanol maser transitions including 6.181 GHz, a transition not included in the comprehensive list of predicted methanol maser transitions in Cragg et al. (2005). Here we report two new methanol maser transitions, 12.229 and 20.347 GHz while searching 86 transitions; neither are included in the list in Cragg et al. (2005). Not only are these never-before-seen methanol maser transitions but the former is brighter than all our other transitions reported here, $S_{12.229}(\text{peak}) > S_{12.178}(\text{peak}) > S_{6.668}(\text{peak})$. The latter is also strong, $S_{6.668}(\text{peak}) > S_{20.347}(\text{peak}) > S_{23.121}(\text{peak})$. We detected no emission in ten hydroxyl transitions (nor the single formaldehyde transition we searched) in any epoch.

A variety of physical conditions can produce transitions with detectable masers as described in Cragg, Sobolev & Godfrey (2002) and Cragg et al. (2005). Since these new maser transitions have never been searched for before, we can only speculate on their rarity. It is not certain if these are even class II methanol maser transitions. Regardless, the conditions for methanol maser activity in G358.93−0.03 are possibly very unique. At the very least to predict a regime in which $S_{12.178}(\text{peak}) > S_{6.668}(\text{peak})$ may also be one in which these other transitions can become inverted and generate maser emission. As noted above, this occurs when the specific column density of methanol is high (Cragg et al. 2005). Such a condition might exist if these masers are located more deeply in the parental cloud where the gas and dust densities will be higher. The higher number density of hydrogen would explain why no hydroxyl masers were detected; Cragg et al. (2002) propose that for number densities of hydrogen in the range $10^5 < n_H < 10^{8.3}$ cm^{-3} hydroxyl and methanol masers are expected. It is hoped that these data, and including the monitoring observations, will avail a better understanding of the variation of the masers as the flare evolves. We will expand upon this topic in our follow-up paper where our monitoring results are presented (MacLeod et al., in preparation).

4.3 An accretion event?

To date there are only two known accretion events that were accompanied by significant maser flaring and the discovery of rare masers. Direct evidence of an accretion event was first reported by Caratti o Garatti et al. (2017) in the HMYSO S255IR-NIRS3; they presented flaring in the near-infrared (NIR) and mid-infrared continuum, while Liu et al. (2018) found submillimeter flaring. Fujisawa et al. (2015) found an associated 6.668 GHz methanol maser flaring event in S255IR-NIRS3, which was characterized in detail by Szymczak et al. (2018). Hunter et al. (2017) proposed an accretion event as the progenitor in NGC 6334I from their detection of a sudden increase in the (sub)millimeter dust emission luminosity (a factor of ∼70). Again this event was accompanied by major flaring in ten maser transitions of three separate molecules, including some very rare, e.g. 4.660 GHz OH and 23.121 GHz methanol (MacLeod et al. 2018).

Thus far the masers in each transition associated with G358.93−0.03 appear to be varying contemporaneously at similar velocities, see Fig. 1. They have brightened significantly, by factors of hundreds and in days to weeks, and some are rare or never-before-detected masers. Dissimilar to the above two other HMYSOs, this source has no associated hydroxyl and only weak water maser emission. Perhaps the energy release during an accretion event is sufficient to energize the masers here and drive the rapid flaring, but the transitions with associated masers are a result of the conditions in which the coherent columns of gas reside.

The idea that protostellar luminosity outbursts are associated with class II methanol masers is supported by modelling that suggests the masers are pumped by infrared radiation (Cragg et al. 2005). However, we did not detect a NIR flare counterpart and nor did (Brogan et al. 2019) find evidence of an increase in the dust emission at millimetre wavelengths. Perhaps the exciting source which provides the pumping IR radiation is deeply embedded, similar to NGC 6334I, and its flare had subsided before observations could be made. Above we find maser modelling requires higher hydrogen number densities to explain the masers detected; the relative strengths of masers reported here may support this argument. Recent simulations (Meyer et al. 2019) indicate that during the early stages of HMYSO evolution, bursts often come in groups of successive events occurring sequentially. However, as HMYSO growth continues, the progression in envelope consumption/dispersal will eventually suppress the gravitational disc instability (Vorobyov & Basu 2015). Thus, NGC 6334I-type accretion bursts are expected to be more frequent than those resembling that of S255IR-NIRS3. If this amazing flaring event in G358.93−0.03 is the result of accretion on to the HMYSO, then it is the first to be detected solely by maser monitoring.

It is difficult to explain the cause of these very fast, strong methanol masers and at these new transitions. The possibility of a rapid increase in the maser pumping efficiency that is accompanied by only small changes in continuum emission should be explored akin to the arguments put forward in Sobolev et al. (1997). Another possibility might be superradiance as described by Rajabi et al. (2019) pertaining to the flaring methanol masers associated with S255IR-NIRS3. It is not clear what best describes the conditions of the maser environment nor this rapid variation presented here. Further insight will likely be gained through future analysis of the ongoing single dish light curves, including a more accurate determination of time lags, along with a detailed comparison of the interferometric images of each transition.

5 SUMMARY AND FUTURE WORK

We confirm that the 6.668 GHz methanol masers associated with G358.93−0.03 are flaring on a time-scale of days as was found in Sugiyama et al. (2019). We report the detection of new associated 12.178 GHz methanol masers that are stronger than the associated 6.668 GHz masers. These masers are accompanied by only the fourth 23.121 GHz methanol maser and two never-before-detected methanol masers at 12.229 and 20.347 GHz; this increases the number of rare methanol maser transitions detected towards G358.93−0.03. The brightest 12.178 GHz channel increased by a factor of over 700 in just 50 d. All of the other transitions also experienced significant flaring activity that occurred on time-scales of days to weeks similar to the associated 6.668 GHz masers. We estimate that there is a time lag, $\tau = 22 \pm 8$ d, between the two brightest velocity channels. Lastly, we detect no NIR flare counterpart.

Revealing the cause for this extraordinary flaring activity is important for the interpretation of class II methanol flares in general. While it has been shown that these flares are signposts of accretion bursts, other excitation mechanisms might be at work as well. This enigmatic source will require interferometric observations and at many transitions, along with monitoring, to determine its nature.

ACKNOWLEDGEMENTS

We thank Dr. Sugiyama for notifying the Maser Monitoring Organisation (M2O) about this exciting source and Dr. Jonathan Quick for his efforts to schedule time around various other observing programmes at HartRAO. I personally thank A&D Stoneworks for the generous time off to work on this manuscript. This research has made use of the VizieR photometric viewer, CDS, Strasbourg, France and the SAO/NASA Astrophysics Data System (ADS). We acknowledge the acceptance of our DDT time request by the director of MPIA. The National Radio Astronomy Observatory is a facility of the National Science Foundation operated under agreement by the Associated Universities, Inc. The Australia Telescope Compact Array is part of the Australia Telescope National Facility which is funded by the Australian Government for operation as a National Facility managed by CSIRO.

REFERENCES

Audard M. et al., 2014, in Beuther H., Klessen R. S., Dullemond C. P., Henning T., eds, Protostars and Planets VI. University of Arizona Press, Tucson, p. 387
Breen S. L., Ellingsen S. P., Caswell J. L., Green J. A., Voronkov M. A., Fuller G. A., Quinn L. J., Avison A., 2012, MNRAS, 421, 1703
Breen S. L., Ellingsen S. P., Contreras Y., Green J. A., Caswell J. L., Stevens J. B., Dawson J. R., Voronkov M. A., 2013, MNRAS, 435, 524
Breen S. L., Sobolev A. M., Kaczmarek J. F., Ellingsen S. P., McCarthy T. P., Voronkov M. A., 2019, ApJ, 876, L25
Brogan C. L. et al., 2019, ApJ, 881, L39
Caratti o Garatti A. et al., 2017, Nat. phys., 13, 276
Caswell J. L. et al., 2010, MNRAS, 404, 1029
Chipman A., Ellingsen S. P., Sobolev A. M., Cragg D. M., 2016, Publ. Astron. Soc. Aust., 33, e056
Contreras Y. et al., 2013, A&A, 549, A45
Cragg D. M., Sobolev A. M., Ellingsen S. P., Caswell J. L., Godfrey P. D., Salii S. V., Dodson R. G., 2001, MNRAS, 323, 939
Cragg D. M., Sobolev A. M., Godfrey P. D., 2002, MNRAS, 331, 521
Cragg D. M., Sobolev A. M., Godfrey P. D., 2005, MNRAS, 360, 533
Ellingsen S. P., Breen S. L., Sobolev A. M., Voronkov M. A., Caswell J. L., Lo N., 2011, ApJ, 742, 109
Fujisawa K., Yonekura Y., Sugiyama K., Horiuchi H., Hayashi T., Hachisuka K., Matsumoto N., Niinuma K., 2015, Astron. Telegram, 8286, 1
Geballe T. R., Lambrides E., Schlegelmilch B., Yeh S. C. C., Goto M., Westrick C., Oka T., Najarro F., 2019, ApJ, 872, 103
Greiner J. et al., 2008, PASP, 120, 405
Hartmann L., Kenyon S. J., 1996, ARA&A, 34, 207
Herbig G. H., 1977, ApJ, 217, 693
Herbig G. H., 1989, in Reipurth B., ed., European Southern Observatory Conference and Workshop Proceedings Vol. 33, European Southern Observatory Conference and Workshop Proceedings. ESO, München, Germany, p. 233
Hu B., Menten K. M., Wu Y., Bartkiewicz A., Rygl K., Reid M. J., Urquhart J. S., Zheng X., 2016, ApJ, 833, 18
Hunter T. R. et al., 2017, ApJ, 837, L29
Krühler T. et al., 2008, ApJ, 685, 376
Liu S.-Y., Su Y.-N., Zinchenko I., Wang K.-S., Wang Y., 2018, ApJ, 863, L12
Lovas F. J., 2004, J. Phys. Chem. Ref. Data, 33, 177
MacLeod G. C. et al., 2018, MNRAS, 478, 1077
Menten K. M., Batrla W., 1989, ApJ, 341, 839
Meyer D. M.-A., Vorobyov E. I., Elbakyan V. G., Stecklum B., Eislöffel J., Sobolev A. M., 2019, MNRAS, 482, 5459
Minniti D., Lucas P., VVV Team, 2017, VizieR Online Data Catalog, 2348
Müller H. S. P., Schlöder F., Stutzki J., Winnewisser G., 2005, J. Mol. Struct., 742, 215
Ott M., Witzel A., Quirrenbach A., Krichbaum T. P., Standke K. J., Schalinski C. J., Hummel C. A., 1994, A&A, 284, 331
Pickett H. M., Poynter R. L., Cohen E. A., Delitsky M. L., Pearson J. C., Müller H. S. P., 1998, J. Quant. Spec. Radiat. Transf., 60, 883
Qiao H., Li J., Shen Z., Chen X., Zheng X., 2014, MNRAS, 441, 3137
Rajabi F., Houde M., Bartkiewicz A., Olech M., Szymczak M., Wolak P., 2019, MNRAS, 484, 1590
Remijan A. J., Markwick-Kemper A., ALMA Working Group on Spectral Line Frequencies, 2007, American Astronomical Society Meeting Abstracts, 39, 963
Rickert M., Yusef-Zadeh F., Ott J., 2019, MNRAS, 482, 5349
Rosolowsky E. et al., 2010, ApJS, 188, 123
Sault R. J., Teuben P. J., Wright M. C. H., 1995, in Shaw R. A., Payne H. E., Hayes J. J. E., eds, ASP Conf. Ser. Vol. 77, Astronomical Data Analysis Software and Systems IV. Astron. Soc. Pac., San Francisco, p. 433
Sobolev A. M., Deguchi S., 1994, A&A, 291, 569
Sobolev A. M., Cragg D. M., Godfrey P. D., 1997, MNRAS, 288, L39
Sugiyama K., Saito Y., Yonekura Y., Momose M., 2019, Astron. Telegram, 12446, 1
Szymczak M., Olech M., Wolak P., Gérard E., Bartkiewicz A., 2018, A&A, 617, A80
Titmarsh A. M., Ellingsen S. P., Breen S. L., Caswell J. L., Voronkov M. A., 2016, MNRAS, 459, 157
Urquhart J. S. et al., 2013, MNRAS, 431, 1752
Vorobyov E. I., Basu S., 2015, ApJ, 805, 115
Wilson W. E. et al., 2011, MNRAS, 416, 832
Wilson T. L., Walmsley C. M., Snyder L. E., Jewell P. R., 1984, A&A, 134, L7

APPENDIX: FREQUENCY SEARCH LIST

We searched transitions of OH (10), H_2CO (1), $CH_3{}^{18}OH$ (2), and CH_3OH (79) in which we found no emission. The results are presented in Table A1.

Table A1. List of transitions searched for associated masers with G358.93−0.03 but not detected.

Freq. (GHz)	Transition Energy level	Velocity Info. $V_{coverage}$ (km s^{-1})	$V_{resolution}$ (km s^{-1})	Observation date	3σ RMS (Jy)
Hydroxyl (OH)					
1.61223101[1]	N = 1$^-$ ⟶ 1$^+$, J = 3/2⟶3/2, F = 1 ⟶ 2	47	0.091	2019 Feb 16	2.0
1.66540184[1]	N = 1$^-$ ⟶ 1$^+$, J = 3/2⟶3/2, F = 1 ⟶ 1	45	0.088	2019 Feb 20	5.0
1.66735903[1]	N = 1$^-$ ⟶ 1$^+$, J = 3/2⟶3/2, F = 2 ⟶ 2	45	0.088	2019 Feb 17	4.0
1.72052998[1]	N = 1$^-$ ⟶ 1$^+$, J = 3/2⟶3/2, F = 2 ⟶ 1	44	0.085	2019 Feb 16	2.0
4.660242[1]	N = 1$^+$ ⟶ 1$^-$, J = 1/2⟶1/2, F = 0 ⟶ 1	32	0.063	2019 Mar 21	0.5
4.765562[1]	N = 1$^-$ ⟶ 1$^+$, J = 1/2⟶1/2, F = 1 ⟶ 0	32	0.061	2019 Mar 11	1.0
6.016746[1]	N = 2$^+$ ⟶ 2$^-$, J = 5/2⟶5/2, F = 2 ⟶ 3	25	0.049	2019 Mar 25	1.0
6.030747[1]	N = 2$^+$ ⟶ 2$^-$, J = 5/2⟶5/2, F = 2 ⟶ 2	24	0.049	2019 Mar 11	4.0
6.035092[1]	N = 2$^+$ ⟶ 2$^-$, J = 5/2⟶5/2, F = 3 ⟶ 3	24	0.049	2019 Mar 11	4.0
6.049084[1]	N = 2$^+$ ⟶ 2$^-$, J = 5/2⟶5/2, F = 3 ⟶ 2	24	0.048	2019 Mar 27	1.5
Formaldehyde (H_2CO)					
4.829659[2]	1(1,0) ⟶ 1(1,1), F = 2 ⟶ 2	30	0.061	2019 Feb 17	1.0
Methanol ($CH_3{}^{18}OH$)					
1.617244[2]	18_5 ⟶ 18_9 A$^+$ (v_t = 1 → 0)	45	0.088	2019 May 16	3.0
1.654342[2]	22_2 ⟶ 22_2 A$^+$ (v_t = 1)	45	0.088	2019 May 17	3.0
Methanol (CH_3OH)					
4.797547[3]	28_2 ⟶ 28_2 A^{-+}, (v_t = 1)	32	0.061	2019 Mar 14	2.0
4.912974[3]	35_2 ⟶ 35_1 E (v_t = 0)	34	0.060	2019 Mar 14	2.0
4.9552[3]	25_4 ⟶ 26_1 A$^-$ (v_t = 0)	34	0.059	2019 Mar 14	2.0
5.005302[3]	3_1 ⟶ 3_1 A^{-+} (v_t = 0)	34	0.058	2019 Mar 12	2.0
5.091373[3]	7_1 ⟶ 7_1 A^{-+} (v_t = 2)	34	0.058	2019 Mar 14	2.0
6.107493[3]	35_4 ⟶ 36_1 A$^+$ (v_t = 0)	34	0.048	2019 Mar 14	2.0
6.27083[3]	30_2 ⟶ 30_2 A^{-+} (v_t = 1)	34	0.047	2019 Mar 14	2.0
6.328305[3]	11_1 ⟶ 11_1 A^{-+} (v_t = 1)	34	0.046	2019 Mar 15	2.0
6.335727[3]	37_{15} ⟶ 36_{14} A^{+-} (v_t = 1 ⟶ 2)	34	0.046	2019 Mar 14	2.0
6.429225[3]	19_4 ⟶ 18_3 A$^+$ (v_t = 2)	34	0.046	2019 Mar 14	2.0
6.543733[3]	8_1 ⟶ 8_1 A^{-+} (v_t = 2)	34	0.045	2019 Mar 14	2.0
6.745123[3]	25_3 ⟶ 25_3 A^{-+} (v_t = 0)	34	0.043	2019 Mar 14	3.0
6.758772[3]	36_4 ⟶ 36_4 A^{+-} (v_t = 0)	34	0.043	2019 Mar 15	3.0
6.785303[3]	28_5 ⟶ 28_9 A$^+$ (v_t = 1 ⟶ 0)	34	0.043	2019 Mar 15	3.0
8.176405[3]	9_1 ⟶ 9_1 A^{-+} (v_t = 2)	34	0.036	2019 Mar 14	2.0
8.254164[3]	37_4 ⟶ 37_4 A^{+-} (v_t = 0)	34	0.036	2019 Mar 14	2.0
8.34159[3]	4_1 ⟶ 4_1 A^{-+} (v_t = 0)	34	0.036	2019 Mar 12	1.0
8.465756[3]	26_3 ⟶ 26_3 A^{-+} (v_t = 0)	34	0.035	2019 Mar 14	2.0
8.467421[3]	6_2 ⟶ 5_{-1} E (v_t = 1)	34	0.035	2019 Mar 14	2.0
8.511071[3]	38_{102} ⟶ 37_{103} E (v_t = 1)	34	0.034	2019 Mar 14	2.0
8.523464[3]	29_4 ⟶ 28_1 A$^+$ (v_t = 1)	34	0.034	2019 Mar 14	2.0
8.655609[3]	17_2 ⟶ 17_2 A^{+-} (v_t = 0)	34	0.034	2019 Mar 14	2.0
8.710622[3]	13_1 ⟶ 13_1 A^{-+} (v_t = 1)	34	0.034	2019 Mar 14	2.0
8.724144[3]	40_{13} ⟶ 39_{14} E (v_t = 2)	34	0.034	2019 Mar 14	2.0
8.845018[3]	15_5 ⟶ 14_7 E (v_t = 2)	35	0.033	2019 Mar 14	2.0
8.856425[3]	26_4 ⟶ 27_5 A$^-$ (v_t = 1)	34	0.033	2019 Mar 14	2.0
8.859549[3]	26_4 ⟶ 27_5 A$^+$ (v_t = 1)	34	0.033	2019 Mar 14	2.0
11.842485[3]	32_2 ⟶ 32_1 E (v_t = 0)	34	0.049	2019 Mar 14	2.0
11.964007[3]	33_{16} ⟶ 34_{13} E (v_t = 0 ⟶ 1)	35	0.049	2019 Mar 14	4.0
11.980899[3]	11_1 ⟶ 11_1 A^{-+} (v_t = 2)	34	0.049	2019 Mar 14	3.0
12.058717[3]	39_4 ⟶ 39_4 A^{+-} (v_t = 0)	34	0.049	2019 Mar 14	3.0
12.329348[3]	16_5 ⟶ 17_4 E (v_t = 0)	34	0.048	2019 Mar 14	2.0
12.347739[2]	25_5 ⟶ 24_6 A$^+$ (v_t = 0)	34	0.047	2019 Mar 14	3.0
12.351[2]	25_5 ⟶ 24_6 A$^-$ (v_t = 0)	34	0.047	2019 Mar 14	3.0
19.9673961[1]	2_1 ⟶ 3_0 E (v_t = 0)	60	0.117	2019 Mar 08	4.0
20.171205[3]	11_1 ⟶ 10_2 A$^+$ (v_t = 0)	59	0.116	2019 Mar 04	4.0
20.182358[3]	22_5 ⟶ 22_9 A$^+$ (v_t = 1 ⟶ 0)	59	0.116	2019 Mar 17	3.0
20.204441[3]	39_{-2} ⟶ 40_{-5} E (v_t = 2 ⟶ 1)	59	0.116	2019 Mar 17	2.0
20.407849[3]	11_3 ⟶ 10_1 A$^+$ (v_t = 2)	59	0.116	2019 Mar 16	4.0
20.908817[3]	16_{-4} ⟶ 15_{-5} E (v_t = 0)	57	0.112	2019 Mar 12	3.0
21.146747[3]	8_2 ⟶ 7_3 E (v_t = 1)	56	0.111	2019 Mar 17	3.0
21.169082[3]	18_9 ⟶ 19_{10} E (v_t = 2)	56	0.111	2019 Mar 17	2.0
21.184378[3]	24_{-4} ⟶ 25_{-2} E (v_t = 0)	56	0.111	2019 Mar 16	3.0

Table A1 – *continued*

Freq. (GHz)	Transition Energy level	Velocity Info. $V_{coverage}$ (km s^{-1})	$V_{resolution}$ (km s^{-1})	Observation date	3σ RMS (Jy)
21.26472[3]	$15_3 \longrightarrow 16_1$ A$^+$ ($v_t = 0$)	56	0.110	2019 Mar 16	3.0
21.281616[3]	$19_{16} \longrightarrow 18_{18}$ E ($v_t = 1 \longrightarrow 0$)	56	0.110	2019 Mar 16	3.0
21.295299[3]	$31_{15} \longrightarrow 30_{18}$ E ($v_t = 2 \longrightarrow 1$)	56	0.110	2019 Mar 18	2.0
21.326889[3]	$10_{-9} \longrightarrow 11_{-8}$ E ($v_t = 2$)	56	0.110	2019 Mar 18	3.0
21.443345[3]	$13_6 \longrightarrow 12_3$ E ($v_t = 1 \longrightarrow 2$)	56	0.109	2019 Mar 18	6.0
21.692261[3]	$36_4 \longrightarrow 37_{-3}$ E ($v_t = 1$)	55	0.109	2019 Mar 18	2.0
21.727015[3]	$33_5 \longrightarrow 33_9$ A$^+$ ($v_t = 1 \longrightarrow 0$)	55	0.108	2019 Mar 18	2.0
21.844244[3]	$28_0 \longrightarrow 27_{-2}$ E ($v_t = 1$)	55	0.107	2019 Mar 18	3.0
21.888175[3]	$21_1 \longrightarrow 21_2$ A^{-+} ($v_t = 1$)	55	0.107	2019 Mar 18	2.0
21.932058[3]	$19_2 \longrightarrow 18_4$ A$^-$ ($v_t = 0$)	54	0.107	2019 Mar 18	3.0
22.019094[3]	$11_3 \longrightarrow 10_5$ A$^+$ ($v_t = 1$)	54	0.106	2019 Mar 18	3.0
22.111687[3]	$25_{-5} \longrightarrow 26_{-3}$ E ($v_t = 0$)	54	0.106	2019 Mar 18	4.0
22.200055[3]	$32_{17} \longrightarrow 31_{19}$ A^{+-} ($v_t = 1 \longrightarrow 0$)	54	0.106	2019 Mar 18	3.0
22.3012[3]	$31_{101} \longrightarrow 30_{103}$ E ($v_t = 2$)	54	0.105	2019 Mar 18	3.0
22.313354[3]	$5_{-3} \longrightarrow 6_3$ E ($v_t = 0$)	54	0.105	2019 Mar 12	3.0
22.365338[3]	$34_{10} \longrightarrow 35_{10}$ E ($v_t = 2 \longrightarrow 1$)	54	0.105	2019 Mar 18	3.0
22.644249[2]	$21_5 \longrightarrow 21_9$ A$^+$ ($v_t = 1 \longrightarrow 0$)	53	0.103	2019 Mar 18	4.0
22.756066[3]	$22_2 \longrightarrow 23_{-1}$ E ($v_t = 2$)	52	0.103	2019 Mar 18	4.0
22.845931[3]	$36_{11} \longrightarrow 35_9$ A^{+-} ($v_t = 0 \longrightarrow 1$)	52	0.103	2019 Mar 18	4.0
22.880797[3]	$15_2 \longrightarrow 16_0$ A$^+$ ($v_t = 0$)	52	0.103	2019 Mar 18	3.0
22.895592[3]	$10_0 \longrightarrow 9_{-3}$ E ($v_t = 1$)	52	0.103	2019 Mar 18	3.0
23.029665[3]	$30_{19} \longrightarrow 31_{17}$ A^{+-} ($v_t = 0 \longrightarrow 1$)	52	0.103	2019 Mar 18	4.0
23.18141[3]	$31_3 \longrightarrow 31_3$ A^{-+} ($v_t = 0$)	52	0.101	2019 Mar 18	5.0
23.200283[3]	$22_2 \longrightarrow 22_2$ A^{+-} ($v_t = 0$)	52	0.101	2019 Mar 18	3.0
23.346879[3]	$7_1 \longrightarrow 7_1$ A^{-+} ($v_t = 0$)	52	0.100	2019 Mar 17	4.0
23.38721[3]	$10_3 \longrightarrow 11_1$ E ($v_t = 0$)	51	0.100	2019 Mar 12	4.0
23.779232[3]	$27_6 \longrightarrow 28_8$ E ($v_t = 1 \longrightarrow 0$)	51	0.099	2019 Mar 18	6.0
23.83718[3]	$13_8 \longrightarrow 14_5$ A$^+$ ($v_t = 2$)	50	0.098	2019 Mar 18	7.0
23.903763[3]	$29_{103} \longrightarrow 30_{101}$ E ($v_t = 2$)	50	0.098	2019 Mar 18	5.0
23.932191[3]	$22_1 \longrightarrow 22_1$ A^{-+} ($v_t = 1$)	50	0.098	2019 Mar 18	4.0
24.013368[3]	$23_7 \longrightarrow 22_8$ A$^+$ ($v_t = 1$)	50	0.097	2019 Mar 18	6.0
24.125963[3]	$34_5 \longrightarrow 33_8$ E ($v_t = 2 \longrightarrow 1$)	50	0.097	2019 Mar 18	7.0
24.153611[3]	$30_{106} \longrightarrow 29_{107}$ E ($v_t = 1$)	50	0.097	2019 Mar 18	10.0
24.218554[3]	$15_5 \longrightarrow 14_8$ A$^+$ ($v_t = 2$)	50	0.097	2019 Mar 18	5.0

Notes. [1]from Lovas (2004), [2]from the CDMS (Müller et al. 2005), [3]from the JPL (Pickett et al. 1998), [4]from Cragg et al. (2005)

[1]*The University of Western Ontario, 1151 Richmond Street, London, ON N6A 3K7, Canada*
[2]*Hartebeesthoek Radio Astronomy Observatory, PO Box 443, Krugersdorp 1741, South Africa*
[3]*Mizusawa VLBI Observatory, National Astronomical Observatory of Japan (NAOJ), 2-21-1 Osawa, Mitaka, Tokyo 181-8588, Japan*
[4]*NRAO, 520 Edgemont Rd, Charlottesville, VA 22903, USA*
[5]*Netherlands Institute for Radio Astronomy, ASTRON, NL-7991 PD Dwingeloo, the Netherlands*
[6]*Sydney Institute for Astronomy (SIfA), School of Physics, University of Sydney, NSW 2006, Australia*
[7]*Korea Astronomy and Space Science Institute, 776 Daedeokdae-ro, Yuseong-gu, Daejeon 34055, Republic of Korea*
[8]*Dublin Institute for Advanced Studies, Astronomy and Astrophysics Section, 31 Fitzwilliam Place, D02 XF86, Dublin 2, Ireland*
[9]*Center for Astrophysics, GuangZhou University, Guangzhou 510006, China*
[10]*Shanghai Astronomical Observatory, Chinese Academy of Sciences, 80 Nandan Road, Shanghai 200030, China*
[11]*Space Research Unit, Physics Department, North West University, Potchefstroom 2520, South Africa*
[12]*Department of Physics and Astronomy, Faculty of Physical Sciences, University of Nigeria, Carver Building, 1 University Road, 410001, Nsukka Nigeria*
[13]*CSIRO Astronomy and Space Science, CSIRO Parkes Observatory, PO Box 276 Parkes, NSW 2870, Australia*
[14]*Max Planck Institute for Astronomy, Königstuhl 17, D-69117 Heidelberg, Germany*
[15]*Institute for Quantum Computing and Department of Physics and Astronomy, The University of Waterloo, 200 University Ave. West, Waterloo, Ontario N2L 3G1, Canada*
[16]*Perimeter Institute for Theoretical Physics, Waterloo, ON N2L 2Y5, Canada*
[17]*Center for Astronomy, Ibaraki University, 2-1-1 Bunkyo, Mito, Ibaraki 310-8512, Japan*
[18]*Thüringer Landessternwarte, Sternwarte 5, D-07778 Tautenburg, Germany*
[19]*Astronomical Observatory, Institute for Natural Sciences and Mathematics, Ural Federal University, 19 Mira street, Ekaterinburg 620002, Russia*

This paper has been typeset from a TEX/LATEX file prepared by the author.